LUND UNIVERSITY

Pore-scale analysis of diffusion transport parameters in digitally reconstructed SOFC anodes with gradient porosity in the main flow direction

Espinoza-Andaluz, M.; Sundén, B.; Andersson, M.

Pore-scale Analysis of Diffusion Transport Parameters in Digitally Reconstructed SOFC Anodes with Gradient Porosity in the Main Flow Direction

M. Espinoza-Andaluz[a,b], B. Sundén[a], and M. Andersson[a,c]

[a]Department of Energy Sciences, Lund University, Lund, SE-221 00, Sweden
[b]Escuela Superior Politécnica del Litoral, ESPOL
P.O. Box 09-01-5863 Guayaquil, Ecuador
[c]Forschungszentrum Jülich GmbH, Institute of Energy and Climate Research, IEK-3
Electrochemical Process Engineering, 52425 Jülich, Germany

One of the promising devices to obtain electrical and thermal energy with considerable high efficiency is the solid oxide fuel cell (SOFC). The electrical energy is the result of the electrochemical reactions that occur inside the fuel cell (FC) when the reactant gases reach the so-called three-phase boundary (TPB). The non-homogeneous and anisotropic characteristics of the layer between the gas channel and the TPB region require a pore-scale analysis to understand the effect of microstructural configurations. The purpose of this paper is to provide understanding of the behavior of the fluid flow through the digitally reconstructed SOFC anodes, with gradient porosity in the main flow direction, using the lattice Boltzmann method (LBM). The impact of the porosity distribution over the fluid behavior is determined for different digitally created SOFC anodes. The SOFC anodes are analyzed keeping the total porosity constant, but varying the local porosity in the flow direction. The impact of a gradient porosity over the gas-phase tortuosity and the normalized effective diffusion coefficient are presented.

Introduction

A fuel cell (FC) is a compact and soundless device that converts the chemical energy presents in the fuel into electrical energy, heat and water; therefore, no polluting gases are emitted to the atmosphere when the energy conversion is carried out. Due to these advantages, the production, development and utilization of FC systems has been increased during the last years. The Fuel Cell Technologies Market Report 2014 showed that the number of FC systems shipped around the world has increased in recent years (1). Nevertheless, there are still some limitations related to the cost and availability of materials involved in the manufacturing process. These limitations can be addressed if a complete understanding of the mechanical, physical and chemical phenomena that occur during the energy conversion is achieved. These phenomena are indeed of a complex nature, mainly due to the interaction between gases and porous materials, electrochemical reactions and, depending on the FC type, phase-change (2-4).

From a simplified point of view, a FC is constituted by an electrolyte sandwiched with two electrodes, i.e., anode and cathode. The FCs that have been attracting major

attention for research are the solid oxide fuel cell (SOFC) and the proton exchange fuel cell (PEFC). This is because both are most widely used in a variety of applications around the world, i.e., stationary power, transportation and portable applications. While SOFCs normally work at higher temperatures (600-800°C), PEFC systems work at considerably lower temperatures (60-80°C) (5).

Considering the aim of the current study, more detailed information about SOFCs is given. The most common architecture for a planar SOFC is the anode supported one, i.e., the thickness of the anode is relatively large in comparison with the cathode and electrolyte. The primary function of the anode is to allow the flow and distribute the gases to facilitate the oxidation of the hydrogen (H_2), or other fuels with hydrogen as a constitutive element (6). At the same time, the oxygen (O_2) is reduced at the cathode side. The anode solid material assists to conduct the free electrons coming from the electrochemical reactions in the three-phase boundary (TPB) to the current collectors.

Because of the high temperatures required during the energy conversion process, and the suitable material properties, nickel (Ni) and yttria-stabilized zirconia (YSZ) are used in the SOFC anode manufacture. However, several rare earth elements used in the manufacturing process are considered as potentially critical in the near- and medium term (7). Therefore, a deep study of the microstructural configuration of the porous materials, i.e., anode and cathode, will allow us to improve the fluid behavior of the reactants.

Considering that measuring microstructural characteristics of a SOFC anode is not only a difficult task, but also expensive because of the equipment required; FC modeling plays an important role in the prediction, design and manufacturing process of FC systems. Several solving methodologies, e.g., smoothed particle hydrodynamics (SPH), dissipative particle dynamics (DPD), Lattice Boltzmann method (LBM), etc., micro-and mesoscale modeling have offered different solutions to obtain detailed information. Among the aforementioned methodologies, the LBM appears as a powerful tool to solve problems in complex geometries such as those found in porous electrodes in SOFCs, and in gas diffusion layers in PEFCs (8,10).

Based on the study presented by Maxwell (11) to determine the electrical conductivity of a medium, it can be concluded that the diffusion phenomena in porous media, such as in SOFC electrodes, depend on the porosity. Additionally, several studies show that the effective diffusion coefficient is highly dependent on the porosity and gas-phase tortuosity (12,13). Given the importance of the mentioned variables for the transport phenomena inside the SOFC, they are studied in the current work.

The purpose of this paper is to analyze the behavior of the fluid, as well as transport parameters such as porosity, gas-phase tortuosity and diffusibility for different porosity distributions in modeled SOFC anodes. The main objective of this study is to propose a design of an SOFC anode, in which for the same amount of composite material, by just varying the microstructural configuration, the reactant gases can more easily reach the TPB. The porosity distribution is obtained by an in-house code, and the fluid behavior is mimicked by the LBM. The local porosity, gas-phase tortuosity and diffusibility are obtained for each simulated SOFC anode and compared with previous studies (14,15).

Methodology

The methodology of this study can be divided into three main parts, the porous media generation, the simulation of the fluid through the porous media representing the SOFC anodes and the computation of the parameters. Once the porous media have been generated, the fluid behavior is simulated by the LBM, and with the obtained results the different parameters are computed. Before going into details of the porous media generation, which represent the SOFC anodes, and the LBM applied, definitions of the computed parameters are given.

Analyzed Parameters

Porosity. The porosity is the ratio between the pore volume, i.e., the void space that can be occupied by the fluid, and the total volume. It can be determined as follows:

$$\varepsilon = \frac{V_g}{V_T} \qquad [1]$$

where V_g is the pore volume occupied by the gas, and V_T represents the total volume. The porosity by definition is a dimensionless parameter and it can be expressed as a percentage. The porosity in SOFC electrodes varies between 0.32 and 0.76, see (16), (17).

Gas-Phase Tortuosity. The gas-phase tortuosity is a measure of the complexity of the medium. This variable is defined as the ratio between the actual flow pathway followed by the gas over the shortest pathway. In several studies the gas-phase tortuosity is approximated by the Bruggeman relationship; (18,19). However, as presented in the study by Navobati and Sousa (20) and considering that in the current study the velocity field through the porous media is determined, this parameter is computed as:

$$\tau_g = \frac{\sum_{i,j,k} \boldsymbol{u}_{mag}(i,j,k)}{\sum_{i,j,k} |\boldsymbol{u}_y(i,j,k)|} \qquad [2]$$

where $\boldsymbol{u}_{mag}$ is the velocity magnitude evaluated in each position, and $\boldsymbol{u}_y$ represents the velocity in the main flow direction. It is a dimensionless parameter, and by definition this parameter is always bigger than unity in porous media.

Diffusibility. The diffusibility is an important parameter describing mass transport phenomena. It is defined as the ratio between the effective diffusion coefficient and the bulk diffusion coefficient. As presented in (9) and (13), this parameter is equivalent to the ratio between the porosity and gas-phase tortuosity:

$$Q = \frac{D^{eff}}{D} = \frac{\varepsilon}{\tau_g} \qquad [3]$$

where Q represents the diffusibility, D^{eff} is the effective diffusion coefficient and D is the bulk diffusion coefficient. Because, in the current study, the mass transport phenomenon is not considered, the right-hand side of Eq. [3] is employed to determine the diffusibility.

Porous SOFC Anode Generation

Five pore domains were modeled to represent the SOFC anode. The total porosity is kept constant, but the local porosity in the main flow direction is varied. On average, the porosity of the digitally generated SOFC anodes is approximately 0.54 based on the values presented in (17). The dimensions of the modeled domains are established considering previous studies (5,21), i.e., 100 x 100 μm as the cross sectional area and 200 μm as thickness.

The pore domain is generated in the through-plane direction, i.e., $y(+)$ direction. The solid and impermeable particles are placed randomly in each cross sectional plane throughout the whole volume. The expected porosities are defined according to the y position, by using a linear function defined as follows:

$$\varepsilon(y) = \left(\frac{\varepsilon_{y=L} - \varepsilon_{y=0}}{N_y - 1}\right) y + \left(\frac{L\, \varepsilon_{y=0} - \varepsilon_{y=L}}{N_y - 1}\right) \quad [4]$$

where N_y represents the number of lattice elements, used in LBM, in the $y(+)$ direction. The porosity of the region near the TPB is defined as $\varepsilon_{y=L}$, and the porosity of the region near the gas flow channels is $\varepsilon_{y=0}$. The lower and upper boundary porosities are determined as 0.34 and 0.74, respectively. These values are interchangeable in order to evaluate porous SOFC anodes with positive and negative porosity gradient. On the other hand, if the porosity is uniformly distributed, $\varepsilon_{y=0}$ and $\varepsilon_{y=L}$ are equal and set to 0.54. Figure 1 shows the trend of the porosity variation along the $y+$ direction for the five different SOFC anodes that are studied in this work.
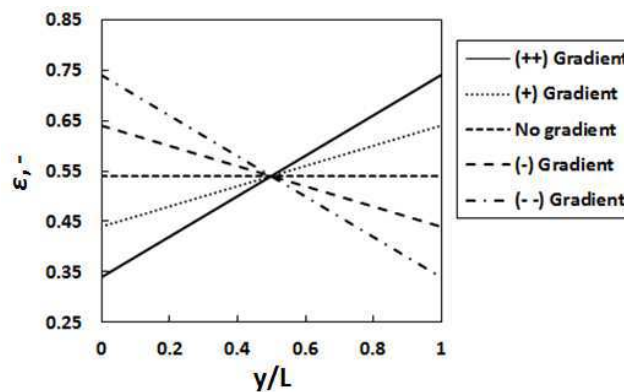

Figure 1. Porosity trend in the cross-plane position for the five modeled domains. For all the domains it is assumed a total porosity equal to 0.54.

Lattice Boltzmann Method

Once the porous media, representing the SOFC anodes, are generated; the fluid behavior through the five domains is mimicked. A primary element of Lattice Boltzmann models is the Boltzmann equation (BE), which is mainly defined as a function of the particle distribution function (PDF). In short, the BE can be expressed as:

$$\frac{\partial f(r,t)}{\partial t} + c \cdot \nabla f(r,t) = \Omega \quad [5]$$

Here, f is the particle distribution function, r the position vector, t the time, and c the velocity vector. In Eq. [5], Ω is the so-called collision operator and it is normally defined as a function of f. Therefore, the collision operator is described as a function of the position and time. Solving Eq. [5] is not an easy task because of the position and velocity dependence of the collision operator (Ω). To simplify the solution, Bhatnagar, Gross and Krook proposed a simplified model to determine the collision operator (22):

$$\Omega = \omega[f^{eq} - f] = \frac{1}{\tau_r}[f^{eq} - f] \qquad [6]$$

where ω is the collision frequency, an important variable to be defined during the modeling of the different transport phenomena. τ_r is the relaxation time, and f^{eq} is the equilibrium distribution function.

Equation [6] is the so-called BGK approximation, and represents the fact that the collision tends to relax to an equilibrium state after the collision step. Using Eqs [5] and [6], and taking into account the nature of the variables, the Lattice Boltzmann equation (LBE) is obtained:

$$\frac{\partial f_a(r,t)}{\partial t} + c_a \nabla f_a(r,t) = \frac{1}{\tau_r}\left[f_a^{eq}(r,t) - f_a(r,t)\right] \qquad [7]$$

In the above equation, a represents each of the discretized directions in which each lattice element has a direct relationship. The equilibrium distribution function (f^{eq}) and the relaxation time (τ_r) should be defined according to the transport phenomena to be solved. The main issue of Eq. [7] is to determine the equilibrium distribution function. Depending on the physical/chemical problem to be solved, the solution of this equation behaves in a different manner. Given the characteristics of the current study, the equilibrium distribution function is determined as (23):

$$f_a^{eq} = \rho \, w_a \left[1 + \frac{c_a \cdot u}{c_s^2} + \frac{(c_a \cdot u)^2}{2 \, c_s^4} - \frac{u^2}{2 \, c_s^2}\right] \qquad [8]$$

Here, ρ is the density, w_a is the weight factor, c_s is the lattice speed of the sound, and u is the macroscopic velocity vector. In the current work, the weighting factors are defined according to the D3Q19 scheme, i.e., nineteen linked velocities between the lattice elements. After the iterative process in which the LBE is solved, the fluid velocity through the pore domain can be obtained by adding, for each lattice node, the product of all the PDFs and the linked velocities. For more detailed information about the methodology, readers are referred to reference (24).

The accuracy and/or convergence of the LBM is in part determined by the right application of the boundary conditions. There are several boundary conditions to obtain the velocity field at the pore - scale level, such as velocity driven, pressure driven or by using second derivative approximations. In the current study, the fluid flow is driven by a pressure difference between the inlet and outlet, and the boundary conditions in these regions were applied according to Zou and He (25). On the remaining four sides of the volume, i.e., the sides parallel to the main flow direction, periodic boundary conditions

are implemented. Because the whole domain is divided in small lattices, each lattice is set as pore or solid material as specified in the following phase function:

$$\phi(x,y,z) = \begin{cases} 0, & x,y,z \in pore\ (white) \\ 1, & x,y,z \in solid\ (black) \end{cases} \qquad [9]$$

All the lattice elements are checked, and when the phase function identifies that a node corresponds to a pore, the LBE is solved. On the other hand, if the analyzed node corresponds to a solid material, no treatment is needed and the bounce-back boundary condition is applied. The pore spaces are assumed to be fully occupied by the fluid and the solid particles are considered as impermeable. Given the iterative nature of the LBM, a convergence criterion should be defined. At each time step, a new velocity field is computed, and the current velocity field is compared with the velocity field in the previous time step. The simulations are stopped using the following criterion:

$$\sum_{i,j,k} \frac{|u^n(i,j,k) - u^{n-1}(i,j,k)|}{|u^n(i,j,k)|} < 10^{-9} \qquad [10]$$

Once the computations are completed, the porosity, gas-phase tortuosity and diffusibility are obtained using the Eqs [1] − [3]. In addition, the local porosity for each SOFC anode is presented, the velocity profile, and the fluid behavior and the relationship to the porosity distribution are analyzed.

Results and Discussion

Porosity values are expected to fall in values according to Eq. [4]. However, to offer a more realistic porous medium, the generated values of this correlation are allowed to vary in ± 5%. It is important to notice that the pore size is a characteristic not considered in this study. However, it will be added in a future more detailed study. The local porosity is computed every 10% of the total SOFC anode thickness and the obtained results are presented in Fig. 2.
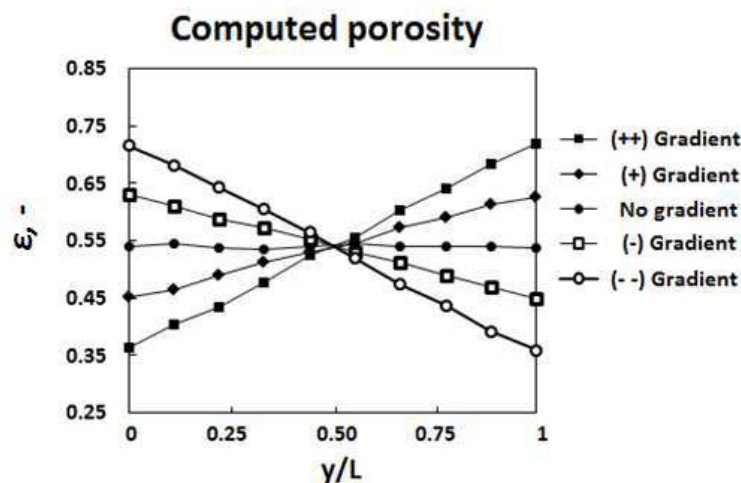

Figure 2. Local porosity for the five modeled SOFC anodes. Each value is obtained every 10% of the total length.

The computed porosity values of the modeled SOFC anodes presented in Fig. 2 show good agreement with the expected ones as shown in Fig. 1. The bulk porosity for each porous domain is also computed and presented in Table I.

TABLE I. Bulk porosity computed from the modeled SOFC anodes

Characteristic	Total porosity
(++) Gradient	0.5397
(+) Gradient	0.5398
No gradient	0.5386
(-) Gradient	0.5401
(- -) Gradient	0.5399

As observed in Table 1, there is no significant variation among the computed porosities of the SOFC anodes. This is because the placing of the solid particles into the domains responds well to Eq. [4]. To visualize the distribution of the solid particles, three modeled porous domains representing the SOFC anodes are depicted in Fig. 3. The selected domains are those in which the solid/pore distribution is most observable. Solid-impermeable particles correspond to the black color while the void spaces are represented by white color.
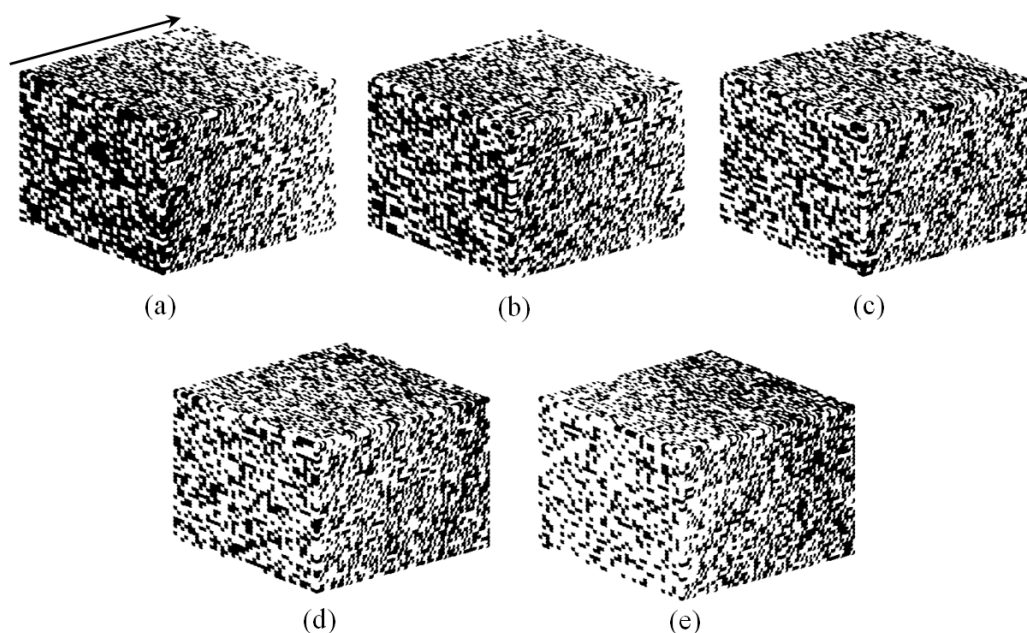

Figure 3. Digitally generated SOFC anodes. Black color regions represent solid particles while white color represents the void spaces. The arrow indicates the main flow direction. (a) Porosity is increasing (++) in the main flow direction, (b) Porosity is increasing (+) in the main flow direction, (c) Porosity is uniformly distributed in the whole domain, (d) Porosity is decreasing (-) in the main flow direction, and (e) Porosity is decreasing (--) in the main flow direction.

As mentioned, according to the phase-function, i.e., Eq. [9], the LBM is solved in the pore spaces and the corresponding boundary conditions are applied. It is assumed that the fluid can full-fill the void spaces in the pore domains, and the iterative steps continue until the steady state is reached based on the convergence criterion. Figure 4 shows the fluid behavior reflected in the mid-plane, height-plane and lateral view for all the digitally created SOFC anodes.
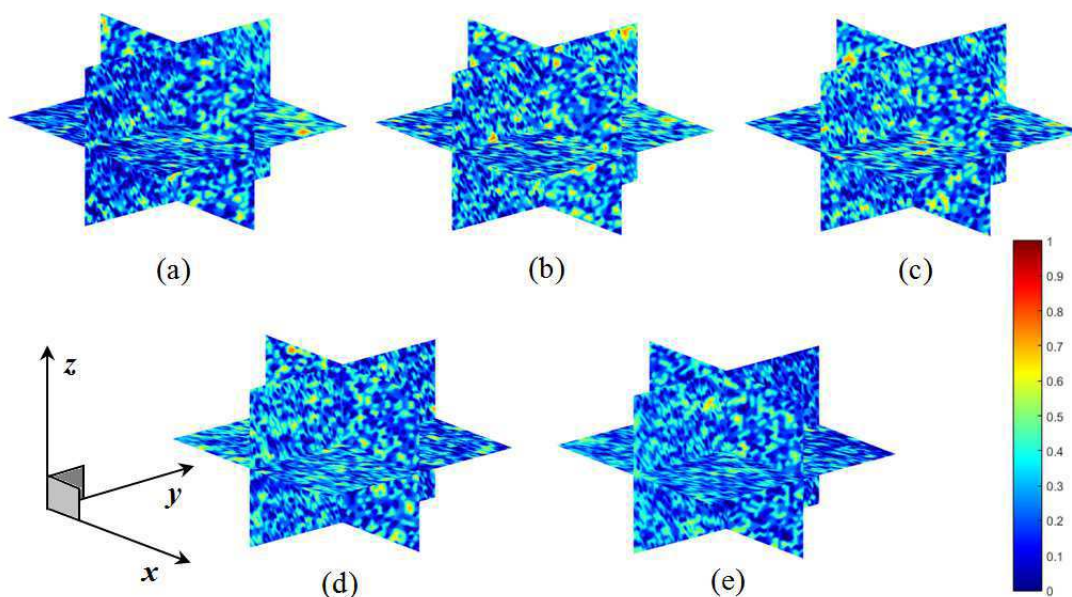
Figure 4. Fluid flow behavior through the digitally created SOFC anodes. The main flow direction is established in *y(+)*. (a) Velocity field when porosity is increasing (++) in the main flow direction, (b) Velocity field when porosity is increasing (+) in the main flow direction, (c) Velocity field when porosity is uniformly distributed in the whole domain, (d) Velocity field when porosity is decreasing (-) in the main flow direction, and (e) Velocity field when porosity is decreasing (--) in the main flow direction

As expected, the recovered fluid flows show the incidence of the gradient porosity along the *y(+)* direction. In the regions in which there is lower porosity, i.e., inlet region in Fig. 4.a and outlet region in Fig. 4.e, there is more presence of lattice nodes with zero velocity. A more detailed analysis of velocity values is presented later in this study.

Based on the obtained velocity field through the porous media, the gas-phase tortuosity values of the SOFC anodes are computed by Eq. [2]. As mentioned, the gas-phase tortuosity is a measure of the complexity of the porous media, and is commonly related to the porosity of the medium. Table II shows the porosity and gas-phase tortuosity values for the digitally created SOFC anodes compared with gas-phase tortuosity values from previous studies available in the open literature.

TABLE II. Porosity and gas-phase tortuosity values compared to previous studies

Porosity distribution	Gas-phase tortuosity computed (τ_g)	Deviation error of gas-phase tortuosity values compared to previous studies (26)	(27)
(++) Gradient porosity	1.337	-1.78%	+2.19%
(+) Gradient porosity	1.353	-0.59%	+3.42%
No gradient porosity	1.353	-0.74%	+3.30%
(-) Gradient porosity	1.348	-0.94%	+3.05%
(- -) Gradient porosity	1.339	-1.61%	+2.36%

In (26), the proposed tortuosity-porosity relationship is the widely known Bruggeman approximation, whereas in (27) the relationship is a logarithmic function obtained when

the porous media are formed of overlapping spheres. Comparing the gas-phase tortuosity values computed in the present study with those obtained by using Bruggeman relationship, i.e., replacing the porosity in the mentioned relationship, it is clear that the Bruggeman relationship overestimates the gas-phase tortuosity values. At the same time, the relationship proposed by Akanni et al. underestimates the values. However, the results in the current work agreed well with these previous studies because the deviation errors fall into an acceptable range, i.e., lower than 5 %.

Analyzing the computed porosity values (Table I) and the obtained gas-phase tortuosity values (Table II), it is possible to state that the solid particle distribution has no real impact over the gas-phase tortuosity. This is supported by the evaluation of the coefficient of variation, a measure that describes the variability of the data respect to the mean, of the gas-phase tortuosity, which is around 0.50%.

The porosity and gas-phase tortuosity have been computed for each porous domain representing the SOFC anode. According to Eq. [3], the diffusibility can be approximated as the ratio of the two aforementioned parameters. Using the computed values from Table I and Table II, the diffusibilities are obtained. To compare the diffusibity values from this work with previous studies, the computed porosity is replaced in the relationships proposed by Bruggeman (26), and Neale and Nader (28). The deviation errors are presented in the last two columns in Table III.

TABLE III. Computed diffusibility values compared to previous studies

Porosity distribution	Diffusibility (Q)	Deviation error of diffusibility values compared to previous studies	
		[26]	[28]
(++) Gradient porosity	0.4037	+1.81%	-7.99%
(+) Gradient porosity	0.3990	+0.60%	-9.08%
No gradient porosity	0.3981	+0.74%	-9.01%
(-) Gradient porosity	0.4007	+0.95%	-8.75%
(- -) Gradient porosity	0.4032	+1.64%	-8.14%

Based on the deviation errors, the computed diffusibilities agreed in a reasonable manner with the previous relationships, i.e., the deviation errors fall into a range of 10.0%. Again, according to the computed diffusibilities, there is no significant impact of the porosity distribution over this parameter. The coefficient of variation is around 0.55%.

To analyze in detail the fluid behavior through the SOFC anodes, the normalized average velocity is computed and presented together with local porosity values of the SOFC anode along the $y(+)$ direction in Fig. 5. Similar to Fig. 3 and Fig. 4, the velocity profiles for all the digitally generated SOFC anodes are presented.
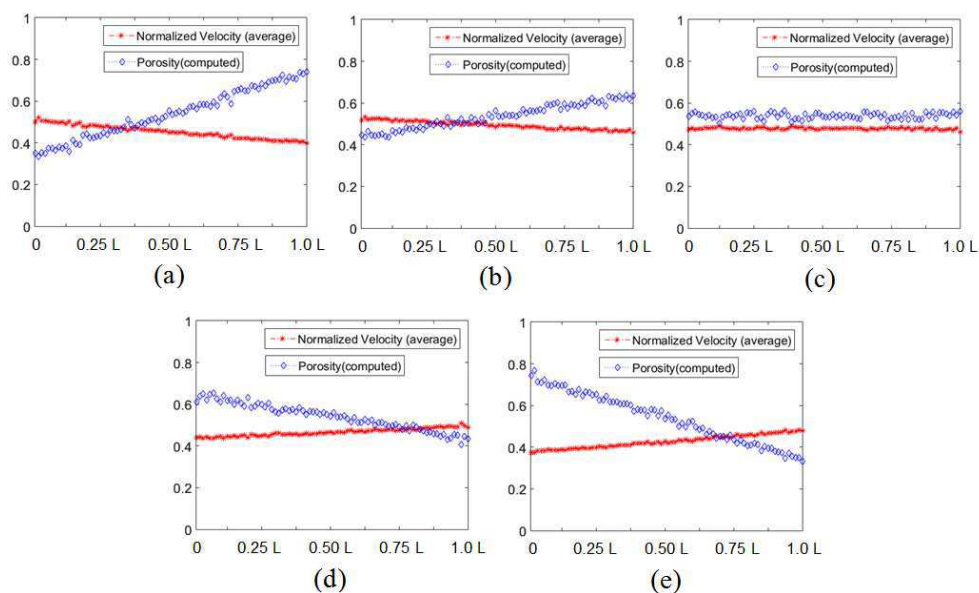
Figure 5. Results of porosity and velocity profile for the digitally created SOFC anodes. (a) Increasing porosity (++) gives decreasing average fluid velocity, (b) Increasing porosity (+) gives decreasing average fluid velocity, (c) Uniform porosity gives uniform average fluid velocity, (d) Decreasing porosity (-) gives increasing average fluid velocity, and (e) Decreasing porosity (--) gives increasing average fluid velocity.

According to the obtained profile velocities, the distribution in which the porosity is decreasing in the flow direction (see Fig. 5.e) gives higher fluid velocities in the TPBs. This would facilitate the contact of the reactant gases with the active sites using the same amount of solid material, and therefore, have influence in the reaction rate during the energy conversion process.

In the present work, the diffusibility is evaluated by using basic transport parameters as porosity and gas-phase tortuosity. However, these results can be compared with the parameters in the center part of Eq. [3]. To obtain the bulk diffusion coefficient and the effective diffusion coefficient, the mass transport phenomena through our modeled SOFC anode should be considered as presented in (29) and (30). The mass transport modeling will help us to understand the impact of the microstructural configuration on the diffusion phenomena in SOFC anodes. However, this is outside the scope of this article and will be considered in a further study.

Conclusions

Five SOFC anodes were modelled with different porosity distributions, keeping the bulk porosity constant. It was found that the porosity distribution has no impact on the gas-phase tortuosity. Considering that in this study the parameters to evaluate diffusibility are the porosity and gas-phase tortuosity, the diffusibility is found not to be affected by the porosity distribution. The obtained velocity profiles through the SOFC anodes show that a decreasing porosity in the main flow direction leads to higher fluid velocities close to the TPBs, and therefore it facilitates the approach of the reactant gases to the active region. However, a deeper analysis of the mass transport phenomena through the SOFC anode is still required.

Acknowledgments

References

1. U. S. Department of Energy, Fuel Cell Technologies Market Report (2014).
2. M. Andersson, S. B. Beale, M. Espinoza, Z. Wu, and W. Lehnert, *Appl. Energy*, **180**, 757-778 (2016).
3. M. Espinoza, M. Andersson, and B. Sundén, *Int. J. Energy Res.*, **41**, 565-578 (2017).
4. T. S. Li, M. Xu, C. Gao, B. Wang, X. Liu, B. Li, and W. G. Wang, *J. Power Sources*, **258**, 1–4 (2014).
5. M. Espinoza, B. Sundén, and M. Andersson, *In ASME 2014 International Mechanical Engineering Congress and Exposition*, V06AT07A058-V06AT07A058 (2014).
6. M. Andersson, J. Yuan, and B. Sundén, *Appl. Energy*, **87**(5), 1461–1476, (2010).
7. U.S. Department of Energy, Solid Oxide Fuel Cells and Critical Materials: A Review of Implications (2011).
8. H. Xu and Z. Dang, *Appl. Energy*, **178**, 294–307 (2016).
9. M. Espinoza, B. Sunden, and M. Andersson, *ECS Trans*, **75**(14), 521–530 (2016).
10. M. Espinoza-Andaluz, M. Andersson, and B. Sundén, *Energy Procedia*, **105C**, 1333 - 1339 (2017).
11. J. C. Maxwell, *A Treatise on Electricity and Magnetism*, p. 403, Clarendon Press, London (1881).
12. W. Kong, Q. Zhang, X. Xu, and D. Chen, *Energies*, **8**(12), 13953–13959 (2015).
13. J. Yuan and B. Sundén, *Int. J. Heat Mass Transfer*, **69**, 358–374 (2014).
14. L. Shen and Z. Chen, *Chem. Eng. Sci.*, **62**(14), 3748–3755 (2007).
15. J. van Brakel and P. M. Heertjes, *Int. J. Heat Mass Transfer*, **17**(9), 1093–1103 (1974).
16. M. Yan, M. Zeng, Q. Chen, and Q. Wang, *Appl. Energy*, **97**, 754–762 (2012).
17. F. Zhao and A. Virkar, *J. Power Sources*, **141**(1), 79–95 (2005).
18. P. K. Das, X. Li, and Z.-S. Liu, *Appl. Energy*, **87**(9), 2785–2796 (2010).
19. K. Zheng and M. Ni, *Sci. Bulletin*, **61**(1), 78–85 (2016).
20. A. Nabovati and A. C. M. Sousa, *New Trends in Fluid Mechanics Research*, 518–521 (2007).
21. A. P. Jamale, C. H. Bhosale, and L. D. Jadhav, *J. Mater. Sci.*, **27**(1), 795–799 (2015).
22. P. L. Bhatnagar, E. P. Gross, and M. Krook, *Phys. Rev.*, **94**(3), 511–525 (1954).
23. Y. H. Qian, D. D'Humières, and P. Lallemand, *Europhys. Lett.*, **17**(6), 479–484 (1992).
24. A. A. Mohamad, *Lattice Boltzmann Method: Fundamentals and Engineering Applications with Computer Codes*, Springer-Verlag, London (2011).
25. Q. Zou and X. He, *Phys. Fluids*, **9**(6), 1591–1598 (1997).

26. D. A. G. Bruggeman, *Ann. Phys.*, **416**(8), 665–679 (1935).
27. K. A. Akanni, J. W. Evans, and I. S. Abramson, *Chem. Eng. Sci.*, **42**(8), 1945–1954 (1987).
28. G. H. Neale and W. K. Nader, *AIChE J.*, **19**(1), 112–119 (1973).
29. T. Gebäck, M. Marucci, C. Boissier, J. Arnehed, and A. Heintz, *J. Phys. Chem. B*, **119**(16), 5220–5227 (2015).
30. M. Espinoza-Andaluz, M. Andersson, and B. Sundén, *Int. J. Hydrogen Energy*, Article in Press (2017). http://dx.doi.org/10.1016/j.ijhydene.2017.02.096.